Suplemento de la Revista Mexicana de Física **4** 021107 (2023) 1–8

A measurement of the mass of the τ lepton using new methods to study semi-invisible decays

J. A. Colorado-Caicedo and E. De La Cruz-Burelo

Physics Department, CINVESTAV IPN,
Av. IPN 2508, San Pedro Zacatenco, Mexico City, 07360, Mexico.

Received 20 April 2023; accepted 25 May 2023

Measuring the mass of particles whose decay products cannot be detected poses a significant challenge due to the complexity of reconstructing these decays and measuring various parameters. However, studying processes involving undetectable particles is crucial as it enables us to delve deeper into familiar decays involving energy loss, such as Standard Model processes involving neutrinos. Additionally, it provides an opportunity to test models associated with physics beyond the Standard Model that can be generated in leptonic colliders. In this study, the mass of the tau lepton was determined by comparing three different methods for decays with semi-invisible final states. Specifically, the measurement focused on the decay $\tau^- \to \pi^- \nu_\tau$ (signal). Among the three methods employed, the most accurate result was obtained using the M_{min} method, yielding a tau lepton mass value of $M_\tau = 1777.06 \pm 0.44$ MeV. The measurement utilized official Monte Carlo data provided by the Belle II collaboration, specifically from the MC13a campaign conducted until 2020, with an integrated luminosity of $100 fb^{-1}$.

Keywords: τ lepton mass; methods to study invisible particles; lepton colliders.

DOI: https://doi.org/10.31349/SuplRevMexFis.4.021107

1. Introduction

The τ lepton is a fundamental particle in the Standard Model of particle physics (SM). There are measurements with extraordinary precision, such as the mass of the electron [1], but the mass of the τ still has a large uncertainty, and its precise mass determination is crucial for testing the theory and exploring physics beyond it. The mass of the tau lepton is an essential parameter for precision electroweak measurements due to its relationship with the weak mixing angle [2], lepton flavor universality tests, including radiative corrections. [3], and the determination of the strong coupling constant α_s at the τ mass scale [4]. Important deviations from the SM in one of these could imply a sighting of BSM physics. Considering the reasons stated above, and the fascinating features of the τ lepton, a better determination of its mass is now essential.

Significant progress has been made in recent years in measuring the mass of the tau lepton. The most accurate measurement recorded in the PDG is 1776.86 ± 0.12 MeV, it is dominated for the fit made by BES III [5] which took advantage of $e^-e^+ \to \tau^-\tau^+$ cross-section near the τ-pairs production threshold, the BaBar [6] and Belle [7] collaborations used the so-called pseudo-mass method (developed by ARGUS [8]) is used to provide the measurement. Currently, the pseudo-mass technique is still employed to determine the mass of the τ in Belle II from the decay mode $\tau^- \to \pi^-\pi^+\pi^-\nu_\tau$, however, the greatest statistic is not concentrated where the pseudo-mass distribution has kinematic fall [9]. The mass of the τ lepton is connected to such a decline. To enhance the precision of mass measurement, the statistics of the distribution used to obtain this quantity must be redistributed around the kinematic edge.

With the purpose of redistributing better the statistics around the point of interest, in this work, we implemented three different methods (M_{edge}, $M_{\min}$ and $M_{\max}$) to study decays where there is lost energy in the final states. Such processes are produced via $e^-e^+ \to X\overline{X}$, where the X could be a heavy particle; consequently, we have the process $X\overline{X} \to (\sum_{i=1}^{n} Y_{ai} + N_1)(\sum_{j=1}^{m} Y_{bj} + N_2)$ where $Y_{a(b)}$ represents any detectable particle and $N_{1(2)}$ a particle that escapes to the detection; processes like these are called semi-invisible decays.

Kinematic edges link the three techniques, and it is possible to create a connection between the kinematic edge and the mass of the mother particle [10, 11]. At the same time, a constraint, that connects the mother particle's masses X and the invisible particles N_1 and N_2, is created. This relationship is useful to suggest novel searching variables for non-standard unseen particles with well-defined initial state energy and momentum, such as in BSM processes [12]; hence, validation in a more practical situation is required. We used these approaches for $e^-e^+ \to \tau^-\tau^+$ followed by $\tau^-\tau^+ \to (\pi^- + \nu_\tau)(\pi^+ + \bar{\nu}_\tau)$, this decay topology is known as (1×1)-prong. We have chosen as signal, and tag a process where τ decays to one pion plus neutrino, just as shown in Fig. 1; there are two challenges here: the first is that neutrinos are impossible to detect entirely, and the second is that τ has a very short lifetime. The combination of these two technical obstacles make reconstructing this process extremely tough. The measurement of the τ mass in the (1×1)-prong topology in the Belle II collaboration has not yet been investigated for the above reasons. We aimed to apply the three approaches indicated above throughout this study to calculate the mass

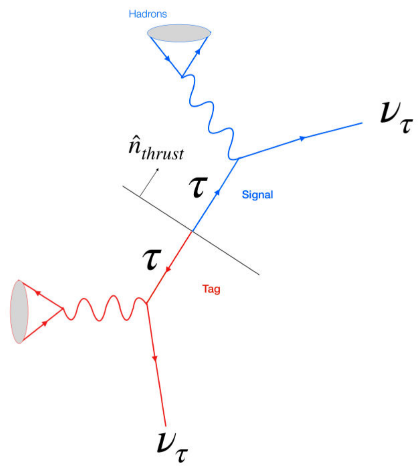

FIGURE 1. Signal-tag scheme in (1×1)-prong topology in tau decay. The direction of the $\hat{n}_{thrust}$ vector that separates the signal from the tag is displayed.

of the τ lepton in the (1×1)-prong topology at the simulation level using official Monte Carlo data from the Belle II experiment for an integrated luminosity of (100 fb^{-1}).

The validation made in this work opens the door for the Belle II collaboration to investigate the mass of the τ utilizing (1×1)-topologies or even to examine BSM processes that satisfy the requirements of the methods used by us.

2. Kinematic reconfiguration

In the extended scenario when we have the decay of the $X\bar{X}$ pair, we choose to start with kinematic equations including eight unknown variables to describe the 4-momentum of two unseen particles, but owing to detector limitations, only six constraint equations are accessible. But, if two parameters, such as the mass of the X and the mass of the N, are introduced, these equations may be solved. As a result, we will count each event with a solution region in the plane composite by the mass of the X particles and the mass of the N particles. Since, in our case we only have for each decay one hadronic particle in the final state that can be detected, we define $h_a \equiv \sum_{i=1}^{n} Y_{ai}$ y $h_b \equiv \sum_{j=1}^{m} Y_{bi}$, the decay topology is illustrated in Fig. 2, where the dotted lines indicate that N1 and N2 escape the detector. We follow the approaches given by Refs. [11, 12]

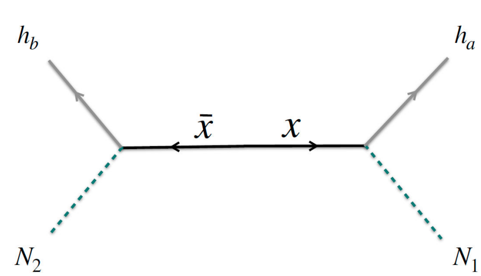

FIGURE 2. Back to back production of the pair $X\bar{X}$ into detectable (Y) and invisible particles (N).

Now, let us now do a kinematic study of the process of Fig. 2. Let P_a, P_b, P_1 and P_2 the 4-momentum of h_a, h_b, N_1 and N_2 in the center-of-mass system (CMS) respectively, where $P_a = (E_a, \mathbf{p_a})$, $P_b = (E_b, \mathbf{p_b})$, $P_1 = (E_1, \mathbf{p_1})$ and $P_2 = (E_2, \mathbf{p_2})$. We have the following kinematic relations due to energy-momentum conservation and invariant mass

$$q^\mu = P_a^\mu + P_b^\mu + P_1^\mu + P_2^\mu, \tag{1}$$

$$P_1^2 = m_1^2, \tag{2}$$

$$P_2^2 = m_2^2, \tag{3}$$

$$(P_a + P_1)^2 = (P_b + P_2)^2 = m_X^2, \tag{4}$$

where $q^\mu = (\sqrt{s}, 0, 0, 0)$ is the 4-momentum in CMS framework, $\mu = 0, 1, 2, 3$; m_1, m_2 and m_X are the masses of N_1, N_2 and X respectively. Note that if our process occurs in a hadronic collider, q^0 and q^3 will be indeterminate, *i.e.*, the first equation will be nonviable; however, in colliders like SuperKEKB, the 4-momentum of the system can be determined, thus P_1^μ and P_2^μ can be fully determined when solving the eight kinematic equations for test values of m_X and m_N.

For simplicity, we redefine the kinematic variables as follows, the normalized energies $z_i \equiv P_i^0/\sqrt{s}$ ($i = 1, 2, a, b, X$), the normalized 3-momentum $\mathbf{k_j} \equiv \mathbf{p_j}/\sqrt{s}$ ($j = 1, 2$), $\mathbf{a} \equiv \mathbf{p_a}/\sqrt{s}$, $\mathbf{b} \equiv \mathbf{p_b}/\sqrt{s}$ and the normalized masses $\mu_k \equiv m_k/\sqrt{s}$ ($k = 1, 2, X, N$). Using the above definitions and the conservation of energy-momentum, the Eqs. (2)-(4) would remain

$$|\mathbf{k_1}|^2 + \mu_1^2 = z_1^2 = (z_X - z_a)^2, \tag{5}$$

$$|\mathbf{k_1} + \mathbf{a} + \mathbf{b}|^2 + \mu_2^2 = (1 - z_a - z_b - z_1)^2, \tag{6}$$

$$|\mathbf{k_1} + \mathbf{a}|^2 + \mu_X^2 = z_X^2, \tag{7}$$

$$|\mathbf{k_1} + \mathbf{a}|^2 + \mu_X^2 = (1 - z_X)^2. \tag{8}$$

As each mother particle takes about half of the energy of the CMS, we may represent the energy of X as $z_X = 1/2$. We need to eliminate $\mathbf{k_1}$ from the kinematic equations; for this, we clear this quantity from the Eq. (5), and we have

$$K \equiv |\mathbf{k_1}|^2 = \left(\frac{1}{2} - z_a\right)^2 - \mu_1^2. \tag{9}$$

To the replacing (9) in (8) we stayed with

$$\mathbf{a} \cdot \mathbf{k_1} = \frac{1}{2}(z_a - z_a^2 - \mu_X^2 + \mu_1^2 - |\mathbf{a}|^2), \tag{10}$$

from (6) we get

$$\mathbf{b} \cdot \mathbf{k_1} = \frac{1}{2}(z_b^2 - z_b + \mu_X^2 - \mu_2^2 - |\mathbf{b}|^2) - \mathbf{a} \cdot \mathbf{b}. \tag{11}$$

If we define

$$A \equiv \mathbf{a} \cdot \mathbf{k_1}, \tag{12}$$

$$B \equiv \mathbf{b} \cdot \mathbf{k_1}, \tag{13}$$

and we develop

$$K(a_z b_y - a_y b_z)^2 = k_{1x}^2 (a_z b_y - a_y b_z)^2 + k_{1y}^2 (a_z b_y - a_y b_z)^2 + k_{1z}^2 (a_z b_y - a_y b_z)^2,$$

we come to the quadratic next expression of k_{1x}^2

$$\begin{aligned}&(Ab_z - Ba_z)^2 + (Ab_y - Bay)^2 \\ &+ 2[(Ab_z - Ba_z)(a_z b_x - a_x b_z) \\ &+ (Ab_y - Ba_y)(a_y b_x - a_x b_y)]k_{1x} \\ &+ |\mathbf{a} \times \mathbf{b}|^2 k_{1x}^2 = 0.\end{aligned}$$

In addition, $\mathbf{k_1}$, $\mathbf{a}$ and $\mathbf{b}$ must comply with

$$\begin{aligned}|\mathbf{k_1} \times \mathbf{a} \times \mathbf{b}|^2 &= |(\mathbf{a} \cdot \mathbf{k_1})\mathbf{b} - (\mathbf{b} \cdot \mathbf{k_1})\mathbf{a}|^2, \\ &= |\mathbf{k_1}|^2 |\mathbf{a} \times \mathbf{b}|^2 \sin^2\theta, \\ &\leq |\mathbf{k_1}|^2 |\mathbf{a} \times \mathbf{b}|^2. \qquad (14)\end{aligned}$$

From the above and using the definitions (12) and (13) we obtain the solution condition for the Eq. (14) in compact form

$$\sqrt{K} \geq \frac{|A\mathbf{b} - B\mathbf{a}|}{|\mathbf{a} \times \mathbf{b}|}. \qquad (15)$$

Developing (15) using the equation (9), and the same time (10) and (11), thus we come to

$$\begin{aligned}&|\mathbf{a} \times \mathbf{b}| \sqrt{\left(\frac{1}{2} - z_a\right)^2 - \mu_1^2} \geq \\ &\left| -\frac{1}{2}\left[(\mu_X^2 - \mu_1^2)\mathbf{b} + (\mu_X^2 - \mu_2^2)\mathbf{a} + \mathbf{H}\right] \right|, \qquad (16)\end{aligned}$$

where

$$\begin{aligned}\mathbf{H} = &(z_b^2 - z_b - |\mathbf{b}|^2 - 2(\mathbf{a} \cdot \mathbf{b}))\mathbf{a} \\ &+ (z_a^2 - z_a + |\mathbf{a}|^2)\mathbf{b}. \qquad (17)\end{aligned}$$

Then, by doing some algebra, we get the following inequality

$$\begin{aligned}&A_1(\mu_X^2 - \mu_1^2)^2 + A_2(\mu_X^2 - \mu_2^2)^2 \\ &+ A_3(\mu_X^2 - \mu_1^2)(\mu_X^2 - \mu_2^2) \\ &+ B_1(\mu_X^2 - \mu_1^2) + B_2(\mu_X^2 - \mu_2^2) \\ &+ C_1\mu_1^2 + D1 \leq 0, \qquad (18)\end{aligned}$$

here

$$A_1 \equiv |\mathbf{b}|^2, \qquad (19)$$

$$A_2 \equiv |\mathbf{a}|^2, \qquad (20)$$

$$A_3 \equiv 2(\mathbf{a} \cdot b), \qquad (21)$$

$$B_1 \equiv 2(\mathbf{b} \cdot H), \qquad (22)$$

$$B_2 \equiv 2(\mathbf{a} \cdot H), \qquad (23)$$

$$C_1 \equiv 4|\mathbf{a} \times \mathbf{b}|^2, \qquad (24)$$

$$D_1 \equiv |\mathbf{H}|^2 - 4|\mathbf{a} \times \mathbf{b}|^2 \left(\frac{1}{2} - z_a\right)^2. \qquad (25)$$

If we consider the case where $\mu_1 = \mu_2$ the Eq. (18) becomes in

$$A_0(\mu_X^2 - \mu_1^2)^2 + B_0(\mu_X^2 - \mu_1^2) + C_0\mu_1^2 + D_0 \leq 0, \qquad (26)$$

where

$$A_0 \equiv |\mathbf{a} + \mathbf{b}|^2, \qquad (27)$$

$$B_0 \equiv 2[\mathbf{a} \cdot \mathbf{H} + \mathbf{b} \cdot \mathbf{H}], \qquad (28)$$

$$C_0 \equiv 4|\mathbf{a} \times \mathbf{b}|^2, \qquad (29)$$

$$D_0 \equiv |\mathbf{H}|^2 - 4|\mathbf{a} \times \mathbf{b}|^2 \left(\frac{1}{2} - z_a\right)^2. \qquad (30)$$

We obtained an equation in which the input variables are the kinematic variables of the particles, we can detect h_a and h_b. It should be noted that the Eq. (26) is an oblique parabola in the plane $(\mu_X^2 - \mu_1^2)$, rather, the solution region is bounded by a parabola (see Fig. 3). All accessible kinematic information for the process $X\bar{X} \to (h_a + N_1)(h_b + N_2)$ is included in the inequalities (18) or (26), depending on whether N_1 and N_2 are distinct or the same kind of particle.

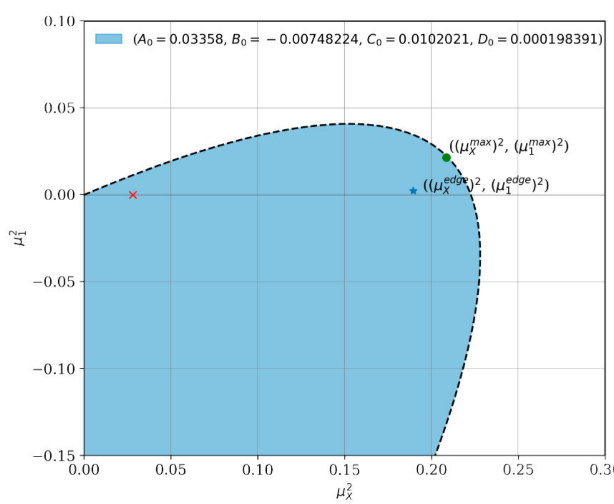

FIGURE 3. The representation of the solution zone from the Eq. (26) for a specific event. The true mass of the τ is displayed as a red cross, the edge mass as a blue star, and the maximum value as a green point. A_0, B_0, C_0 and D_0 were picked from the local simulation.

3. $\mathrm{M_{edge}}$, $\mathrm{M}_{\min}$ and $\mathrm{M}_{\max}$ methods

The equation's parabola (26) is rotated $45°$ in the plane $(\mu_X^2 - \mu_1^2)$. If we apply a rotational transformation where $\theta = 45°$, and put the expression in terms of the new variables ($\mu_X'^2$ and $\mu_1'^2$), we get the parabola vertex in the new reference system, and if we perform the inverse transformation, we get the original system's vertex parabola. This gives us our variables $(\mu_X^{\text{edge}})^2$ and $(\mu_1^{\text{edge}})^2$, which represent the vertex of the parabola in the plane$(\mu_X^2 - \mu_1^2)$. The expressions are

$$(\mu_X^{\text{edge}})^2 = \frac{4B_0^2 + 3C_0^2 - 16A_0D_0 - 8B_0C_0}{16A_0C_0},$$
$$(\mu_1^{\text{edge}})^2 = \frac{4B_0^2 - C_0^2 - 16A_0D_0}{16A_0C_0}. \tag{31}$$

Up to this point, we can have two alternatives, that the parabola has a vertex in quadrant I or that it is in quadrant IV, but if it is in the latter, we will have a restriction on $(\mu_1^{\text{edge}})^2$ and it is that this cannot take negative values, in that case, we will assign the minimum value to this variable, that is, if the vertex is in quadrant IV, the furthest physical point will be the intersection of the parabola and the axis μ_X^2. Hence, from (26) we will obtain for the situation when $\mu_1^2 = 0$

$$(\mu_X^{\text{borde}})^2 = \frac{\sqrt{B_0^2 - 4A_0D_0} - B_0}{2A_0},$$
$$(\mu_1^{\text{borde}})^2 = 0. \tag{32}$$

Both (31) and (32) will be used to extract the masses m_X^{edge} and m_1^{edge} knowing that $m_X^{\text{edge}} = (\mu_X^{\text{edge}})\sqrt{s}$ y $m_1^{\text{edge}} = (\mu_1^{\text{edge}})\sqrt{s}$.

Now, to construct the other two methods, let us begin with the Eq. (18) and let us particularize to the decay $\tau^- \to \pi^-\nu_\tau$. For practicality, let us consider $\mu_1 = \mu_{\nu_\tau}$ and $\mu_X = \mu_\tau$. Assuming $m_{\nu_\tau} = 0$, the Eq. (18) reduces to

$$(A_1 + A_2 + A_3)(\mu_\tau^2)^2 + (B_1 + B_2)(\mu_\tau^2) + D_1$$
$$= A_0(\mu_\tau^2)^2 + B_0(\mu_\tau^2) + D_0 \leq 0. \tag{33}$$

Solving, we obtain

$$(\mu_\tau^2)^2 = \pm\frac{\sqrt{B_0^2 - 4A_0D_0}}{2A_0} - \frac{B_0}{2A_0}, \tag{34}$$

this can be seen as

$$\left(\mu_\tau^{\min}\right)^2 \leq (\mu_\tau)^2 \leq (\mu_\tau^{\max})^2\,, \tag{35}$$

given that $m_\tau = \mu_\tau\sqrt{s}$, thus

$$M_{\min}^2 \leq m_\tau^2 \leq M_{\max}^2, \tag{36}$$

where

$$M_{\min}^2 = \left(\sqrt{s}\right)^2 \left(\frac{-B_0 - \sqrt{B_0^2 - 4A_0D_0}}{2A_0}\right), \tag{37}$$

$$M_{\max}^2 = \left(\sqrt{s}\right)^2 \left(\frac{-B_0 + \sqrt{B_0^2 - 4A_0D_0}}{2A_0}\right). \tag{38}$$

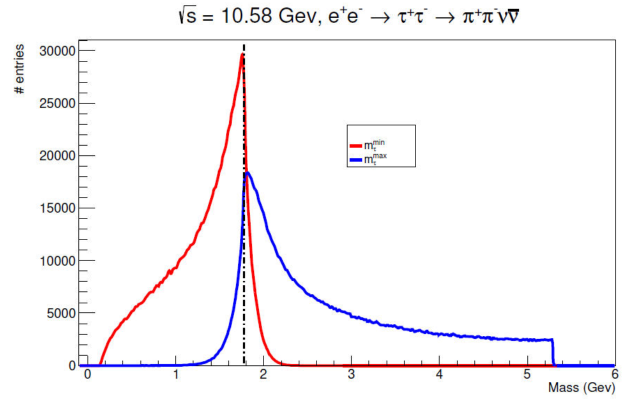

FIGURE 4. The distribution of M_{min} (M_{max}) in red (blue). The dashed line is the true mass m_τ^{true}.

According to (36), the variables $M_{\min}$ and $M_{\max}$ should have endpoints just in the mass of the τ as shown in the Fig. 4. The mass we seek is associated to locations where these distributions have a noticeable rise, as seen in the mass distributions, and it is these points that we will estimate.

4. Event selection

The Belle II detector is composed of several sub-detectors arranged in a cylindrical configuration around e^-e^+ interaction point (IP). We select τ-pair candidates by requiring only two final state charged particles; each was less than 3 cm in the z-direction and less than 1 cm in the transverse plane from the mean IP. By merging the information from all sub-detectors into a global discriminator akin to a probability ratio, the particle in the signal hemisphere must be designated as a pion; such hemisphere is created via $thrust$ that is defined by the unit vector $\hat{u}_{thrust}$ perpendicular to the line separating the signal and tag (see Fig. 1). The value of $thrust$ is defined as $V_{thrust} \equiv \sum_i |\mathbf{p}_i^{cm} \cdot \hat{n}_{thrust}|/|\mathbf{p}_i^{cm}|$, such that said value is the maximum, where $\mathbf{p}_i^{cm}$ is the momentum of each final-state particle in the CMS. The values are split using the vector $\hat{u}_{thrust}$ and the $thrust$. In this manner, we have the production back-to-back of τ-pairs in the CMS. The variable E_{ECL}/p, which is the ratio of the energy deposited in the calorimeter to the momentum of charged particles, requires $0 \leq E_{ECL}/p \leq 0.8$ to ensure that there are more pions in the tracks.

The background where e^-e^+ produce in the final-state $q\bar{q}$ with $q = u, d, s, c$ (hadronic), $l^-l^+\gamma$ (dileptonic), and $e^-e^+l^-l^+$ (two-photon) needs to be reduced. To identify the criterion for suppressing these backgrounds, we employ simulated events. The KKMC generator is used to create the $e^-e^+ \to \tau^-\tau^+$ process [13, 14]. The τ decays are handled with the software TUAOLA [15], their radiative corrections by PHOTOS [16], We use KKMC to simulate $\mu^-\mu^+(\gamma)$ and $q\bar{q}$ production, PYTHIA [17] for the fragmentation of the $q\bar{q}$ pair; BabaYaga@NLO [18–21] for $e^-e^+ \to e^+e^-(\gamma)$ events, AAFH [22–24] and TREPS [25] for the non-radiative

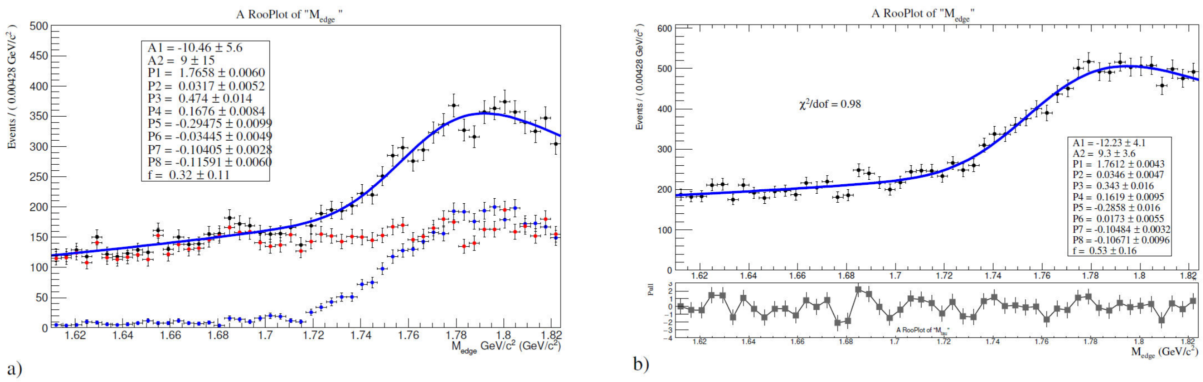

FIGURE 5. a) Signal (blue) and background (red) BDT distributions. b) FOM with maximum in 0.2.

final states $e^-e^+l^-l^+$. The Belle II Software Framework (Basf2) [26] uses Geant4 [27] to simulate the response of the detector to the passage of the particles.

To reduce the background noise caused by $e^-e^-\!\!\rightarrow q\bar{q}$ we required zero neutrals in the final state. The photons utilized for π^0 reconstruction are in clusters with an energy of at least 0.1 GeV. Neutral pions are photon pairs with masses between [115,152] MeV/c2. Events containing photons that meet the aforementioned criteria but are not included in the π^0 reconstruction and have an energy greater than 0.2 GeV are likewise excluded. Imposing a cut in the $Thrust \leq 0.99$ we suppressed events from $e^+e^-(\gamma)$ and $q\bar{q}$.

All other events that are not considered as signal are background, *i.e.*, the remain events of low multiplicity $(ee, ee\mu\mu, \mu\mu, eeee)$, $q\bar{q}$ $(q = u, d, s, c)$, mixed $(B_0\bar{B}_0)$ and charged (B^+B^-). To clean our signal $\tau^- \rightarrow \pi^-\nu_\tau$ (all other decays of the τ are considered as noise), we used a Machine Learning (ML) model based on Boosting Decision Trees (BDT) implemented in ROOT [28] through an environment for the processing and evaluation of multivariate classification such as TMVA (Toolkit for Multivariate Data Analysis) [29]. The new variable "BDT" was optimized with the purpose of extracting the best cut for the separation signal/background using the figure of merit (FOM) $2\left(\sqrt{N_{sig}+N_{bkg}}-\sqrt{N_{bkg}}\right)$, where N_{sig} is the number of the signal events and N_{bkg} is the number of background events.

5. Estimation of the τ mass

5.0.1. M_{edge} *method*

To determine the mass of the τ, we performed a unbinned likelihood fit [30] using the following parametrization

$$F(M_{\text{edge}}) = fS_{PDF} + (1-f)B_{PDF}, \tag{39}$$

where S_{PDF} is the probability density function (PDF) for the signal, B_{PDF} is the PDF for the background and f is a coefficient less than 1 that is subject to the normalization conditions. The empirical PDF for the signal has the following form

$$\begin{aligned} S_{PDF}(M_{\text{edge}}) &= (P_3 + P_4 M_{\text{edge}} + P_6 M_{edge}^2 + P_7 M_{\text{edge}}^3) \\ &\times erf\left(\frac{M_{\text{edge}} - P_1}{P_2}\right) + P_8 M_{\text{edge}}^2 \\ &+ P_5 M_{\text{edge}} + 1, \end{aligned} \tag{40}$$

where P_1 is the estimator for the mass of the τ, the estimator is not exactly the mass of the tau, but it is assumed that it will be a range from the real value, so the value of the estimator must be corrected for the selected function in simulated data; for this, we use an official Monte Carlo sample (MC13a) for the production of τ-pairs, for which we know the generation mass (1777 MeV) that was taken as the real value.

The M_{edge} distribution for the background is flat, it can be modeled as a linear function. The PDF for the background is

$$B_{PDF}(M_{\text{edge}}) = A_1 + A_2 M_{\text{edge}}. \tag{41}$$

For the variable M_{borde} in the mass window $1.610 < M_{\text{edge}} < 1.824$ and using the addition of PDF's a value of the estimator $P_1 = 1765.80 \pm 6.0$ MeV was obtained [Fig. 5a)]. The difference between the estimator and the true mass is $\Delta_m = 11.2$ MeV, and using this bias value, the final estimation in the remaining sample is adjusted [Fig. 5b)]. After correcting for the bias, we obtain a value for the mass of the τ of $m_\tau = 1772.40 \pm 7.38$ MeV. The uncertainties were summed in quadrature for this final value.

5.0.2. $M_{\min}$ *method*

For this estimation, we used the same parametrization function presented above [Eq. (39)] and the same PDF for the background B_{PDF}. The signal PDF is given by

$$\begin{aligned} S_{PDF}(M_{\min}) &= (P_3 + P_4 M_{\min} + P_6 M_{\min}^2 + P_7 M_{\min}^3) \\ &\times erfc\left(\frac{M_{\min} - P_1}{P_2}\right) \\ &+ P_8 M_{\min}^2 + P_5 M_{\min} + 1. \end{aligned} \tag{42}$$

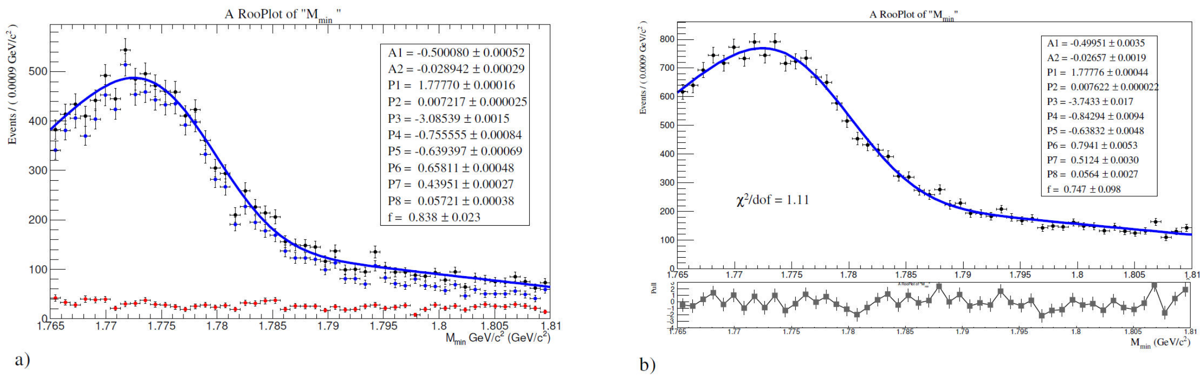

FIGURE 6. a) Signal (blue) and background (red) BDT distributions. b) FOM with maximum in 0.2.

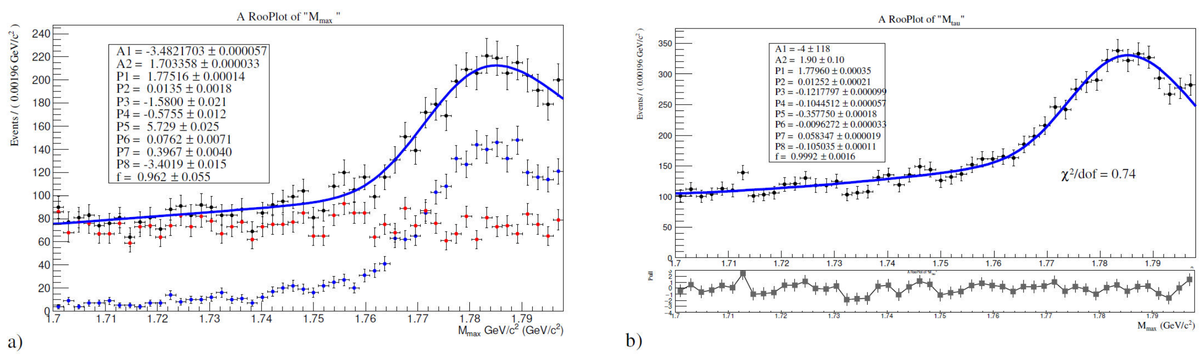

FIGURE 7. a) Signal (blue) and background (red) BDT distributions. b) FOM with a maximum in 0.2.

A value for the estimator of $P_1 = 1777.70 \pm 0.16$ MeV is obtained with a difference from the real value of $\Delta_m = -0.70$ MeV. Already considering the remaining sample [Fig. 6b)], and with bias, we corrected the estimation of the mass to obtain a value for the mass of the τ lepton of $m_\tau = 1777.06 \pm 0.47$ MeV.

5.0.3. $M_{\max}$ method

For the variable $M_{\min}$ we used the same previous parametrization function, and the same signal PDF (40).

In this case, it was possible to obtain a value for the mass estimator of $P_1 = 1775.16 \pm 0.14$ MeV [Fig. 7a)] for a difference in mass of $\Delta_m = 1.84$ MeV. Correcting then with this bias to the value obtained in the adjustment to the remaining data, a value for the mass of $m_\tau = 1781.44 \pm 0.38$ MeV was obtained.

6. Conclusions

Three approaches for measuring tau lepton mass based on the solubility of kinematic equations were adopted in this study. The first is for a full solution zone called M_{edge}, where it was discovered that the density of events is higher towards the point of actual mass. The other two techniques, $M_{\min}$ and $M_{\max}$, used zero mass for the tau neutrino as a rough approximation. The key conclusion is that the $M_{\min}$ approach is the best way for measuring the tau lepton mass in the (1×1)-prong topology (which has not yet been implemented in the Belle II collaboration), yielding a mass for the τ lepton of $m_\tau = 1777.06 \pm 0.47$ MeV. This result is obtained with the official Belle II simulated data in the MC13a campaign. It is crucial to note that the methods utilized in this study to do mass measurements in decays with semi-invisible end products are naturally biased due to the inability of reconstructing those decays in their entirety. Also, it is important to highlight that there is a relation between the precision and the uncertainties of the measurements with the redistribution of the events (without increase data) around the real value of the mass. For instance, the measurement made with the $M_{\min}$ method presents major statistics distributed around the point of interest, and we obtained with this the more accurate measurement with the lower uncertainty. Therefore, looking at the M_{edge} variable we can see that it has the greatest widening in its distribution, thus, it has the largest bias with a value of $\Delta_m = 11.2.$ MeV and the worst accuracy.

Finally, we have verified three approaches for investigating decay processes originating in leptonic colliders with invisible particles in the final state; such processes can be also BSM decays where it is necessary to deploy sophisticate ways to extract new information with the limited variables that the detectors can give us in order to discover new particles or impose competitive production upper bounds.

1. E. Tiesinga *et al*., CODATA recommended values of the fundamental physical constants: 2018, *Rev. Mod. Phys*. **93** (2021) 025010, https://doi.org/10.1103/RevModPhys.93.025010.
2. P. D. Group *et al*., Progress of Theoretical and Experimental Physics *Review of Particle Physics*, **2022** (2022), https://doi.org/10.1093/ptep/ptac097.
3. W. J. Marciano and A. Sirlin, Electroweak radiative corrections to τ decay, *Phys. Rev. Lett*. **61** (1988) 1815, https://doi.org/10.1103/PhysRevLett.61.1815.
4. M. Davier, A. Höcker, and Z. Zhang, The physics of hadronic tau decays, *Rev. Mod. Phys*. **78** (2006) 1043, https://doi.org/10.1103/RevModPhys.78.1043.
5. M. Ablikim, *et al*., Precision measurement of the mass of the τ lepton, *Phys. Rev. D* **90** (2014) 012001, https://doi.org/10.1103/PhysRevD.90.012001.
6. B. Aubert *et al*., Measurements of the τ mass and the mass difference of the τ+ and τ- at BABAR, *Phys. Rev. D* **80** (2009) 092005, https://doi.org/10.1103/PhysRevD.80.092005.
7. K. Belous *et al*., Measurement of the τ Lepton Mass and an Upper Limit on the Mass Difference between τ+ and τ-, *Phys. Rev. Lett.* **99** (2007) 011801, https://doi.org/10.1103/PhysRevLett.99.011801.
8. H. Albrecht *et al*., A measurement of the tau mass, *Physics Letters B* **292** (1992) 221, https://doi.org/10.1016/0370-2693(92)90634-G.
9. Belle II Collaboration, *et al.*, τ lepton mass measurement at Belle II (2020), https://arxiv.org/abs/2008.04665..
10. Q.-F. Xiang, *et al*., Measuring masses in semi-invisible final states at electron-positron colliders, *Phys. Rev. D* **95** (2017) 075037, https://doi.org/10.1103/PhysRevD.95.075037.
11. E. De La Cruz-Burelo, A. De Yta-Hernandez, and M. Hernandez-Villanueva, New method for beyond the Standard Model invisible particle searches in tau lepton decays, *Phys. Rev. D* **102** (2020) 115001, https://doi.org/10.1103/PhysRevD.102.115001.
12. Belle II Collaboration *et al*., Search for lepton-flavor-violating τ decays to a lepton and an invisible boson at Belle II (2022), https://doi.org/10.48550/arXiv.2212.03634.
13. S. Jadach, B. Ward, and Z. Was, The precision Monte Carlo event generator KK for two-fermion final states in e^+e^- collisions, *Computer Physics Communications* **130** (2000) 260, https://doi.org/10.1016/S0010-4655(00)00048-5.
14. S. Jadach, B. Ward, and Z. Wąs, Coherent exclusive exponentiation for precision Monte Carlo calculations, *Phys. Rev. D* **63** (2001) 113009, https://doi.org/10.1103/PhysRevD.63.113009.
15. S. Jadach, J. H. Kühn, and Z. Wąs, TAUOLA - a library of Monte Carlo programs to simulate decays of polarized τ leptons, *Computer Physics Communications* **64** (1991) 275, https://doi.org/10.1016/0010-4655(91)90038-M.
16. E. Barberio, B. van Eijk, and Z. Wąs, Photos-a universal Monte Carlo for QED radiative corrections in decays, *Computer Physics Communications* **66** (1991) 115, https://doi.org/10.1016/0010-4655(91)90012-A.
17. T. Sjöstrand *et al*., An introduction to PYTHIA 8.2, *Computer Physics Communications* **191** (2015) 159, https://doi.org/10.1016/j.cpc.2015.01.024.
18. C. Carloni Calame *et al*., Large-angle Bhabha scattering and luminosity at flavour factories, *Nuclear Physics B* **584** (2000) 459, https://doi.org/10.1016/S0550-3213(00)00356-4.
19. C. Carloni Calame *et al.*, The BABAYAGA event generator, *Nuclear Physics B - Proceedings Supplements* **131** (2004) 48, https://doi.org/10.1016/j.nuclphysbps.2004.02.008.
20. C. M. Carloni Calame, An improved parton shower algorithm in QED, *Physics Letters B* **520** (2001) 16, https://doi.org/10.1016/S0370-2693(01)01108-X.
21. G. Balossini, et al., Matching perturbative and parton shower corrections to Bhabha process at flavour factories, *Nuclear Physics B* **758** (2006) 227, https://doi.org/10.1016/j.nuclphysb.2006.09.022.
22. F. Berends, P. Daverveldt, and R. Kleiss, Radiative corrections to the process $e^+e^- \rightarrow e^+e^+\mu^+\mu^-$, *Nuclear Physics B* **253** (1985) 421, https://doi.org/10.1016/0550-3213(85)90540-1.
23. F. Berends, P. Daverveldt, and R. Kleiss, Complete lowest-order calculations for four-lepton final states in electron-positron collisions, *Nuclear Physics B* **253** (1985) 441, https://doi.org/10.1016/0550-3213(85)90541-3.
24. F. Berends, P. Daverveldt, and R. Kleiss, Monte Carlo simulation of two-photon processes: II: Complete lowest order calculations for four-lepton production processes in electron-positron collisions, *Computer Physics Communications* **40** (1986) 285, https://doi.org/10.1016/0010-4655(86)90115-3.
25. S. Uehara, TREPS: A Monte-Carlo Event Generator for Two-photon Processes at e^+e^- Colliders using an Equivalent Photon Approximation (2013), https://arxiv.org/abs/1310.0157.
26. T. Kuhr *et al*., The Belle II Core Software, Computing and Software for Big Science **3** (2018) 1, https://doi.org/10.1007/s41781-018-0017-9.
27. S. Agostinelli *et al.*, Geant4-a simulation toolkit, *Nucl. Instrum. Meth. A Detectors and Associated Equipment* **506** (2003) 250, https://doi.org/10.1016/S0168-9002(03)01368-8.
28. R. Brun and F. Rademakers, ROOT: An object oriented data analysis framework, Nucl. Instrum. Meth. A **389** (1997) 81, https://doi.org/10.1016/S0168-9002(97)00048-X.

29. A. Hocker *et al*., TMVA - Toolkit for Multivariate Data Analysis (2007) https://doi.org/10.48550/arXiv.physics/0703039.

30. W. Verkerke and D. Kirkby, The RooFit toolkit for data modeling (2003), https://arxiv.org/abs/physics/0306116.